Blind Source Separation in Laser-Induced Breakdown Spectroscopy

1. Abstract

Many years have passed since the birth of laser induced breakdown analysis and several steps forward have been made for the improvement of the technique from a hardware and software point of view. Libs has been skyrocketed, literally. Now, the need to automate the process of recognition, classification and quantification of the analytes becomes more and more pressing. In the chapters of this book, the new advances regarding these issues have been described. Here, an attempt to separate the spectra of the analytes will be described, which uses some of the most common blind source separation techniques. This type of approach is not a usual practice in Libs, so our contribution wants to provide a taste of the potential of this method for anyone who wants to try their hand at analyzing real data.

2. Introduction

A laser-induced emission spectrum is a complex object from the point of view of both the physical meaning of the emission peaks and the amount of information contained within it. Simplifying, a spectrum is a sum of different signals to which noise, depending on different factors, is added. There are several variables that can be extracted from an emission spectrum, whose formal description is referred to previous chapters in this book.

The analyte signal (S) in a laser-induced breakdown spectrum is the light radiation emitted by an analyte at a specific wavelength and collected by a detector. The plasma also emits a signal referred to as continuum background (B) composed of bremsstrahlung radiation from free electrons and recombination emission. With the plasma decay, the emission lines begin to appear and, therefore, to optimize the signal to noise ratio (SNR), the plasma light is collected by a time-resolved detector at times that are generally between a few hundred nanoseconds and a few microseconds (Sun & Yu 2009). Therefore, the detector response (x) at a given wavelength in a single-analyte spectrum is the sum of S, B, and the noise (D) introduced by the detector (dark current, stray light, etc.) (Hahn & Omenetto, 2012; Tognoni & Cristoforetti, 2016):

$$x=S+B+D \quad (1)$$

The subtraction of the continuum background (B) to the analyte signal results in a net analyte signal (Hahn & Omenetto, 2012; Tognoni & Cristoforetti, 2016):

$$x_{net}=x-B \quad (2)$$

This formula is valid for only one analyte. In the most frequent case, the signal (S) will be the sum of the signals of all the analytes present in the material plus their backgrounds. The elimination or correction of the different contributions of these backgrounds is not simple, because their intensity depends on the emission wavelengths, the surface characteristics of the sample and its matrix and, finally, on the conditions of plasma formation (Xu et al., 1997; Tognoni et al, 2002). This means that these parameters are not always fixed, also due to fluctuations in the laser power and differences due to the inhomogeneity of the sample, and leads us to estimate the continuum background spectrum by spectrum and sample by sample, as proposed by many authors (Sun & Yu, 2009; Yaroshchyk & Eberhardt, 2014), or using the msbackadj function of the Matlab bioinformatics toolbox©.

Besides the continuum background, random noise also affects the LIBS signal. Mermet et al. (2008) recognize four main factors contributing to random noise in LIBS spectra: source noise, shot noise, detector noise and thermal drift (Table 1).

Table 1 Four main factors that cause noise in LIBS signals

Noise type	description	intensity	reference
Source noise	shot-to-shot fluctuations in laser energy, rate of ablation, laser-plasma coupling, and plasma characteristics.	Standard deviation proportional to the signal.	(Bauer et al., 1998; Danzer, 1984; Kempenaers et al., 2002; Sallé et al., 2006)
Shot noise	Caused by photons that arrives on the detector (described by Poisson statistics).	Standard deviation proportional to the square root of the signal.	(Mermet et al., 2008)
Detector noise	Fluctuation caused mainly by shot noise plus negligible effects due to the characteristics of the detector	Same as shot noise	(Mermet et al., 2008)
Thermal drift	caused by heating of the laser components and the optical path	Spectrum (thermal) drift	(Mermet et al., 2008)

Bulajic et al. (2002) simulate shot and detector noise in typical libs spectra as Gaussian variables, as also done by Motto-Ros et al. (2019), who remark that, when the line intensities are weak (i.e., close to the background value), the noise can be considered independent of the intensity. Tognoni & Cristoforetti (2016), furthermore, come to the conclusion that the detector noise can be considered negligible. In this chapter, we follow these authors, considering the random noise as Gaussian and signal-independent. A simple correction of the thermal drift in the spectrum can be done using a calibrated lamp.
Let us now consider a 2D map with P pixels (Figure 1), whose generic pixel p is equipped with an entire LIBS spectrum observed at M discrete wavelengths. At each wavelength, the observed spectrum for an N-analyte material has the form

$$x_p(\lambda) = \sum_{i=1}^{N} a_{p,i}\, s_i(\lambda) + n_p(\lambda) \qquad \lambda = \lambda_1, \lambda_2, \ldots, \lambda_M \qquad p = 1,2,\ldots,P \qquad (3)$$

where $s_i(\lambda)$ is the ideal spectrum of the i-th analyte, $a_{p,i}$ is its abundance at point p and n_p is the associated noise. Hence, at each pixel, the measured spectrum is a weighted superposition of the spectra of the fundamental elements, where neither the mixing coefficients nor the element spectra are known.

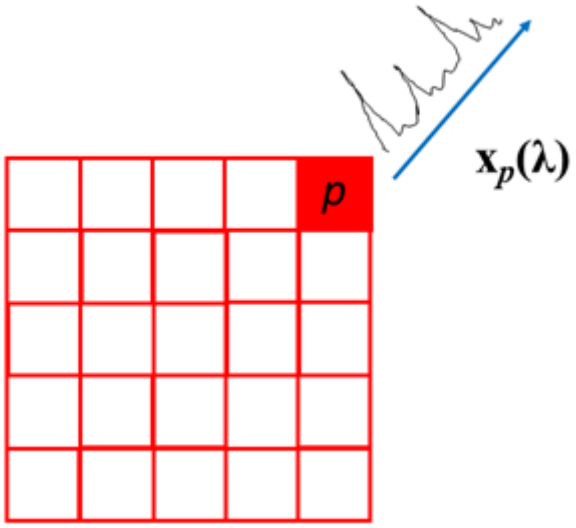

Figure 1 Schematic drawing of a LIBS 2D map.

The first problem to be faced before processing the signals, whether they come from a punctual analysis or from an elementary map, is the elimination or reduction not only of background noise but other types of noise too. Many authors (Alexander et al., 2012; Bauer et al., 1998; Fu et al., 2019; Mermet et al., 2008; Schlenke et al., 2012; Zhang et al., 2013, 2015; Zou et al., 2014) have faced the problem in different ways, some using purely mathematical methods and some trying to give a physical meaning to the operations performed.

A typical libs spectrum is formed by the sum of the emissions of the neutral (I) and first ionization (II) atomic species present in the plasma light captured by the spectrometer. Furthermore, these are associated with the presence of different kinds of interferences, caused by various factors due to the instrument, measurement conditions, plasma physics, etc. The most influential is the continuum background emitted, as said above, by the plasma (see Figure 2).

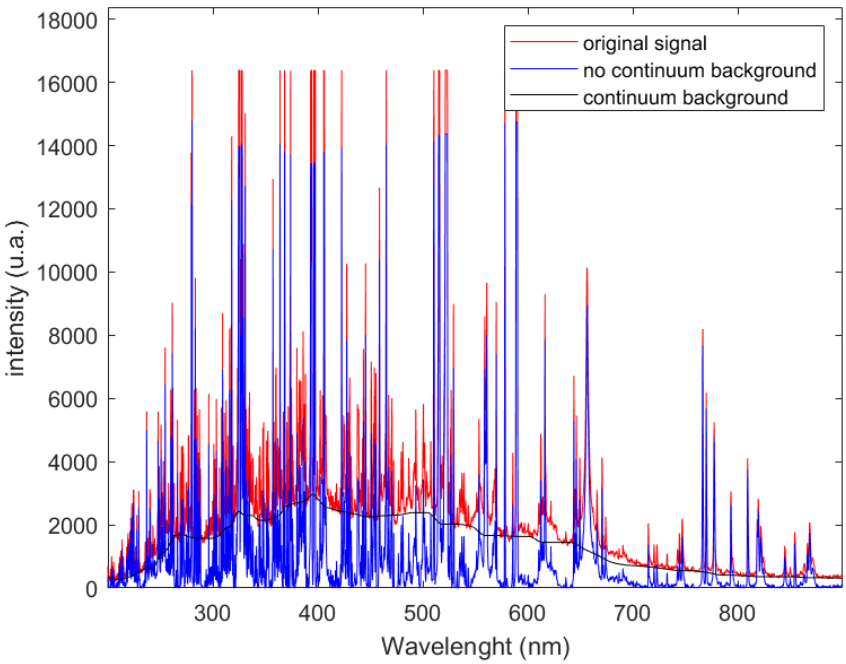

Figure 2 A typical LIBS signal, as output from the spectrometer and corrected for the continuum background.

The simplest and most used method to analyse a LIBS spectrum is to select the wavelengths which the neutral (I) and first ionization (II) analyte emissions correspond to, in a supervised manner (Boué-Bigne, 2008; Busser et al., 2018; Carvalho et al., 2015; Casado-Gavalda et al., 2017; Dixit et al., 2017; Fabre et al., 2018; Fortes et al., 2015; Gimenez et al., 2016; Häkkänen & Korppi-Tommola, 1995; Hausmann et al., 2017; Hoehse et al., 2011; Hong et al., 2014; Kim et al., 1998; Le Guével et al., 2018; Lednev et al., 2017; Lefebvre et al., 2016; Li et al., 2017; López-López et al., 2017; Lopez-Quintas et al., 2012; Motto-Ros et al., 2012; Noll et al., 2001; Pagnotta et al., 2017; Peng et al., 2016; Rifai et al., 2018; Romero & Laserna, 1997; Schiavo et al., 2016; Sheta et al., 2015; Škarková et al., 2017; Sperança et al., 2017; St-Onge et al., 2002; Taparli et al., 2018; Trichard et al., 2018; Wiggins et al., 2013; Xu et al., 2016). This procedure is valid when we know the elemental composition of the analysed material or, in any case, when we have a clear idea of its qualitative composition. In the problematic cases of very noisy signals or presence of elementary peaks that show self-absorption, this method brilliantly bypasses each of these problems by making an *a priori* selection of the best peak lines.

In the analysis of completely unknown samples, consisting of many analytes with highly variable proportions, the supervised selection of analyte peaks attributable to elemental qualitative composition begins to show its negative sides. Specifically, it will be necessary to start considering various other factors such as the signal to noise ratio (SNR), signals that overlap each other and create sums of peaks, various types of noise and, finally, self-absorption.

The continuum background at each spectral line is typically estimated from the signal values measured at the rising and dropping slopes of that line. Usually, the analyte signal is characterized through the intensities of its peaks. These can normally be derived in three ways: the intensity at the central wavelength of each peak, the integral of the signal over the line width or, less frequently, the sum of the signal values along each spectral line.

When the number and type of analytes to be detected in a LIBS spectrum is completely unknown, the use of source separation methods could be of great help: these methods can separate the sources of a signal without any knowledge of its components or how they are mixed. In the literature, there are several methods and examples of algorithms for separating the components of a signal (Choi et al., 2005; Jain & Rai, 2012; Pal et al., 2013); among these, the most interesting are the Principal Component Analysis (PCA) (Karhunen et al., 1998, 1995; Karhunen & Joutsensalo, 1994; Oja, 1995; Oja & Plumbley, 2003; Pajunen & Karhunen, 1997; Zhu et al., 2006), the Minimum Noise Fraction (MNF) (Dabiri & Lang, 2018; Gao et al., 2017; Harris et al., 2005; Luo et al., 2016) and the fast-Independent Component Analysis (FastICA) (Hyvarinen, 1999a, 1999c, 2001; Lin et al., 2007; Sun, 2005).

3. Data model

We consider the emission spectra at the P pixels as a multivariate signal resulting from the sum of individual signals, each describing the characteristics of the LIBS emission of a single element. We can rewrite eq. 3 in matrix form:

$$x(\lambda)=As(\lambda)+n(\lambda) \qquad \lambda= \lambda_1, \lambda_2,\ldots, \lambda_M \qquad (4)$$

where the P-vector x contains all the measured spectra at each wavelength, the N-vector s contains all the elemental spectra, A is a $P \times N$ mixing matrix and the P-vector n contains the noise contributions at each wavelength.

We have said that the analysis of a LIBS map consists in identifying the elements that compose the material under investigation, and their relative abundance at each inspected point. This means estimating s and A from knowledge of x. Even in the case of $P \geq N$ and zero noise, if no additional assumption is made, this problem is clearly underdetermined, since any full-rank choice for A can give

an estimate of s that accounts for the evidence x. Hence, eq. 4 is a particular instance of a problem of blind source separation (BSS) (Cichocki & Amari, 2002). Here, the sources are the spectra of the *N* elements, and the mixtures are the spectra at the *P* measurement points.

4. Analyzing LIBS data via Blind Source Separation

4.1 Second-order BSS

Even if no specific information is available, statistical assumptions can often be made on the sources. In our case, it can be assumed that the spectra of the elements are mutually uncorrelated, and it is intuitively clear why one could decorrelate the input data to try to extract the individual spectra. This amounts to apply second-order statistical techniques to estimate A and s from x.

Let us first pose in the case where the noise in eq. (4) is zero and assume that the data vectors are either zero-mean or zero-centered by preprocessing. We seek for a linear transformation $y(\lambda) = Wx(\lambda)$ such that $<y_i^T y_j>= 0$, $\forall i, j = 1, \ldots, P, i \neq j$, where W is a $P \times P$ matrix and the notation $< \cdot >$ means expectation. In other words, the components of the transformed data vector y are orthogonal. This operation is not unique, since, given an orthonormal basis of a subspace, any further rigid rotation still yields an orthonormal basis of the same subspace. Our data covariance matrix is the $P \times P$ matrix:

$$Cov_x =< xx^T >\approx \frac{1}{M}\sum_{\lambda=\lambda_1}^{\lambda_M} x(\lambda)\, x^T(\lambda) \tag{5}$$

Since the data are usually correlated, matrix Cov_x will be non-diagonal. The covariance matrix of vector y is:

$$Cov_y =< Wxx^T W^T >= WCov_x W^T \tag{6}$$

To obtain an output y with mutually orthogonal components, Cov_y should be diagonal. Let us perform the eigenvalue decomposition of matrix Cov_x, and call V_x the matrix of its eigenvectors, and Λ_x the diagonal matrix of its eigenvalues, sorted in decreasing order. It is easy to verify that both the following choices for W (among possible others) yield a diagonal Cov_y:

$$W_{PCA} = V_x^T \tag{7}$$

$$W_w = \Lambda_x^{-\frac{1}{2}} V_x^T \tag{8}$$

Matrix W_{PCA} produces a set of vectors y_i that are orthogonal to each other and whose Euclidean norms (i.e. their variances) are equal to the eigenvalues of the data covariance matrix. This is the principal components transform, or principal component analysis (PCA) (Cichocki & Amari, 2002). The output principal components are sorted by decreasing values of variance. By using matrix W_w, we obtain a set of orthogonal vectors of unit norms, i.e. mutually orthogonal vectors located on a spherical surface (whitening, or Mahalanobis transform). Other choices for the data decorrelating matrix W can be taken via the multiplication from the left of any whitening matrix by any orthogonal matrix. Being $P \geq N$, and assuming that matrix A is full-rank, all the eigenvalues of order larger than N vanish, and in principle matrix W_w cannot be computed, and the $P \times P$ matrix W_{PCA} has no meaning. Moreover, if $P \gg N$, the problem could also become computationally unmanageable. Equations (7) and (8) maintain their validity if only the first N eigenvalues and eigenvectors of Cov_x are selected, and the size of the PCA and the whitening matrices becomes $N \times P$. Alternatively, the user could choose to guess a number N' of significant analytes and only compute the first N' eigenvalues and eigenvectors. Successively, possible components associated with near-zero eigenvalues can be neglected as non-significant. In the noiseless case, thus, the BSS problem under uncorrelation assumption simply becomes a problem of

eigenvalue analysis. As its solution is not unique, however, the correspondence of the output vectors y_i and the original sources s_i is not ensured theoretically.

4.2 Maximum Noise Fraction

The second-order based Blind Separation Source (BSS) techniques described above have been derived under the noiseless assumption. In practice, the measured data are always more or less noisy. One possibility to face this problem is to try to denoise the data before separation. In remote-sensed multispectral data, it has been observed that PCA is often able to sort the decorrelated data based on quality besides variance. Hence, the most significant extracted components are also somehow less affected by noise. This fact could depend on the high cross-correlation that often exists in multispectral data, which can lead to a compression of information into the low-order principal components. This compression is manifested as a steadily decreasing signal-to-noise ratio as the order of the component increases, i.e. the related eigenvalue decreases. However, there are numerous examples, especially among aircraft scanner data, where this is not the case (Green et al., 1988). Indeed, when the noise variances are unequal in different bands, it may happen that noise contributes significantly to the variance of one of the first components, so that this might actually contain less useful information than another component with lower variance. This is because the principal component transform is sensitive to the scaling of the data to which is applied. To some extent, the scaling (or weighting) of the multispectral bands is arbitrary, and usually equal weighting is applied. A more natural strategy, conversely, is to weight the bands so that the noise level in each of them is the same. Green et al. (1988) exploit this principle to derive a transform based on maximization of SNR, so that the transformed components are ranked by SNR rather than variance as done in PCA. They show that this transform, the maximum noise fraction (MNF) transform, produces uncorrelated components that maximize their noise fraction (or, equivalently, their SNR if taken in reverse order). Then, MNF produces components ordered by image quality. Lee et al. (1990) show that the MNF transform is equivalent to a two stage transformation in which the data are first transformed so that the noise is whitened, i.e. it has unit variance in all bands, and is uncorrelated across the bands, and the second stage is a PCA. This transform has been called Noise Adjusted Principal Component (NAPC) transform. The first stage of NAPC provides a natural weighting where the noise in each band is equal in magnitude and is uncorrelated with the noise in any other. Therefore, in the second stage, maximizing the noise-whitened multispectral data variance with PCA results in maximizing their corresponding SNR. In Roger (1994), a fast computation for NAPC was also proposed. Assuming that the noise and signal components of the data are uncorrelated, the NAPC transform has been formally derived by Lee et al. (1990, p. 297), by using arguments similar to those used in the derivation of the principal component transform, and tracing back the variational problem of maximizing SNR at each subsequent component to that of maximizing variance. The practical NAPC (or MNF) algorithm requires the knowledge of the symmetric, positive definite covariance matrix $\mathrm{Cov_n}$ of the additive noise affecting the data, and consists of the following steps:

1) From Cov_n, compute its eigenvector matrix, V_n, and the diagonal matrix of its eigenvalues Λ_n, such that

$$V_n Cov_n V_n^T = \Lambda_n \tag{10}$$

2) Define a noise-whitening matrix $W_{wn} = \Lambda_n^{-\frac{1}{2}} V_n^T$ for which

$$W_{wn} Cov_n W_{wn}^T = I \tag{11}$$

where I is the identity matrix

3) Transform the data covariance matrix, Cov_x, by W_{wn} to obtain the noise-adjusted data covariance matrix, Cov_x^{adj}:

$$Cov_x^{adj} = W_{wn} Cov_x W_{wn}^T \quad (12)$$

4) From Cov_x^{adj}, compute its eigenvector matrix, U_x, and the diagonal matrix of its eigenvalues, Λ_x^{adj}, such that

$$U_x Cov_x^{adj} U_x^T = \Lambda_x^{adj} \quad (13)$$

5) The MNF components are given by the set of vectors y, produced from the original data vectors x by the transform:

$$y = W_{MNF} x \quad (14)$$

where W_{MNF}, the NAPC-MNF transform matrix, is given by $W_{MNF} = U_x^T \Lambda_n^{-\frac{1}{2}} V_n^T$.
Green et al. (1988) state without proof that the MNF components are the left-hand eigenvectors of $Cov_{\boldsymbol{n}} Cov_{\boldsymbol{x}}^{-1}$, and that the eigenvalues of Λ_x^{adj} are the corresponding noise fraction values. In Roger (1994), it is formally shown that matrix W_{MNF} simultaneously diagonalizes Cov_x and $Cov_{\boldsymbol{n}}$, that is:

$$W_{MNF} Cov_x W_{MNF}^T = \Lambda_x^{adj} \quad (15)$$

And

$$W_{MNF} Cov_{\boldsymbol{n}} W_{MNF}^T = I \quad (16)$$

which implies that the transformed data are uncorrelated and ordered by their variance, i.e. by their SNR. In many situations the covariance matrix of the noise is available. If not, it may be estimated from the covariance of the signal first-order differences (Green et al., 1988). This approximation is more accurate the more regular and smooth the data signals are. Still in (Green et al., 1988), MNF has been analysed in different situations of noise. It is apparent that MNF reduces to PCA for noiseless data (i.e. when Cov_n is taken identically null). However, MNF performs exactly like PCA also in other circumstances. For instance, when noise is uncorrelated with equal variance in all bands, it is straightforward to see that the two procedures produce the same set of eigenvectors. Finally, it is worth noting that MNF can be used for noise reduction. Indeed, once data have been transformed into components with ordered SNR, it is logical to spatially filter the noisiest components and subsequently to transform back to the original coordinate system. As the components that will be filtered by this procedure contain a reduced signal component, the resulting signal degradation will be much less than if the same smoothing were performed on the untransformed data. This procedure should allow much stronger smoothing to be applied, without severe signal degradation. However, since the signal content of even the noisiest MNF component is rarely so low to be overlooked, virtually every MNF component needs to be filtered before re-transformation, which leads back to the typical over-smoothing problems of denoising. In any case, denoising is not the feature of NAPCA-MNF that we are interested in here, where we aim at exploiting its signal separation capabilities.

4.3 Independent Component Analysis

An effective technique used to solve a BSS problem like the LIBS problem of eq. 4 could be the so-called independent component analysis (ICA) technique (Hyvärinen et al., 2001), which assumes full statistical independence of the sources and has been first derived for noise-free data to be then extended

to the realistic noisy case. Unlike the above-reported second-order approaches, the ICA assumptions guarantee the uniqueness of the solution, ensuring that its outputs reproduce the original sources up to arbitrary scaling and permutation.
If the prior distribution for each source is known, independence is equivalent to assume a factorized form for the joint prior distribution of s:

$$\Psi\big(s(\lambda)\big) = \prod_{i=1}^{N} \Psi_i\left(s_i(\lambda)\right) \qquad \forall\lambda \tag{17}$$

The separation problem can be formulated as the maximization of function (17) in A and s, subject to the constraint x= As. This is equivalent to the search for a matrix $W = (w_1, w_2, \ldots, w_N)^T$, such that, when applied to the data $x = (x_1, x_2, \ldots, x_P)$, produces the set of vectors $w_i^T x$ that are maximally independent, and whose distributions are given by the Ψ_i. By taking the logarithm of eq. 17, the problem solved by ICA algorithms is then:

$$\widehat{W} = \arg max_w \sum_{\lambda}\sum_{i} \log \Psi_i\left(w_i^T x(\lambda)\right) + M \log|\det(W)| \tag{18}$$

In the square case P = N, matrix $\widehat{W}$ is an estimate of A^{-1} up to arbitrary scale factors and permutations of the columns. Hence, each vector $\hat{s}_i = \widehat{w}_i^T x$ is one of the original source vectors up to a scale factor. Besides independence, to make separation possible a necessary extra condition for the sources is that they all, but at most one, must be non-Gaussian. To enforce non-Gaussianity, generic super-Gaussian or sub-Gaussian distributions can be used as priors for the sources. These have proven to give very good estimates for the mixing matrix and for the sources as well, no matter of the true source distributions, which, on the other hand, are usually unknown (Bell & Sejnowski, 1995a, 1995b).

4.4 ICA for Noisy data

In Hyvärinen & Oja (1997), a fast-fixed-point algorithm (FastICA) is developed that takes some measure of non-Gaussianity and then finds projections in which this is locally maximized for whitened data. Projections in such directions give consistent estimates of the independent components if the measure of non-Gaussianity is well chosen. In Hyvarinen, (1999b), this approach was taken for deriving a noisy version of the algorithm, based on the availability of measures of non-Gaussianity that are insensitive to Gaussian noise on the data. Specifically, a modification of the fixed-point FastICA algorithm was introduced where Gaussian moments, simply estimated from noisy observations, are used as contrast functions for data affected by Gaussian noise. As for the NAPC transform, also this "noise-adjusted ICA" algorithm assumes knowledge of the covariance matrix of the noise. In the noise-free ICA algorithm, a first step entails the whitening of the data. In the noisy version of the algorithm, the noise is considered by replacing the ordinary whitening, based on the eigenvalue decomposition of the data covariance matrix Cov_x (see eq. 8), with a "quasi-whitening" operation, based on the covariance matrix of the ideal, noise-free mixture, which is given by Cov_x–Cov_n. The quasi-whitened data follow a noisy ICA model as well, with an orthogonal mixing matrix, and easily derivable noise covariance matrix. The quasi-whitened data are then fed into a fixed-point algorithm with Gaussian moments, which uses the covariance matrix of the transformed noise to avoid bias (Hyvarinen, 1999b).

6. Numerical examples

To demonstrate the potential effectiveness of BSS methods in isolating elemental spectra from LIBS measurements, we rely on simulated spectra built from known data and a simplified noise model. In this section, we show and compare the results obtained by MNF and ICA for different signal-to-noise ratios.

Table 2 Simulated relative abundances in 4 measurement points of a non-homogeneous bronze sample

Measurement point	%Cu	%Sn	%Zn	%Pb
#1	83.6	1.9	11.4	3.1
#2	87.1	5.0	5.5	2.4
#3	90.9	0.3	7.8	1.0
#4	84.1	1.4	10.5	4.0

We start from the typical relative abundances (see Table 2) found in a bronze alloy containing copper, tin, zinc and lead. By small random perturbations of these abundances, we simulated the LIBS spectra in 40 measurement points of a non-homogeneous bronze sample. From the NIST LIBS database, (https://physics.nist.gov/PhysRefData/ASD/LIBS/), we retrieved the spectra of the four analytes in the ionization statuses likely to appear when acquired by a spectrometer, that is, Cu I, Sn II, Zn II, Pb I and Pb II (hereafter, the sum of the latter two is denoted by Pb Sum). The chosen spectral range is 200 to 400 nm in air, with 2500 wavelengths per spectrum, electron temperature $T_e = 1eV$ and electron density $N_e = 10^{17} cm^{-3}$. Figure 4 shows these spectra with the line intensities in arbitrary units.

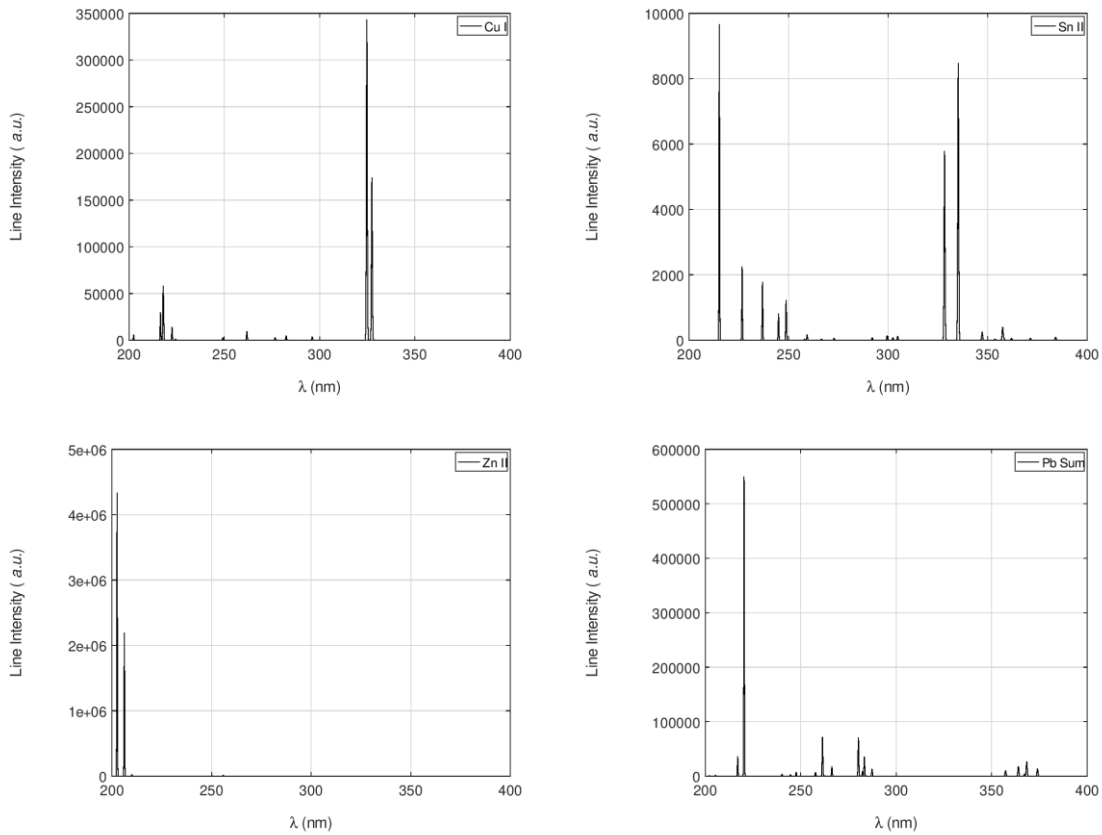

Figure 4 Elemental LIBS spectra as retrieved from the NIST database.

The elemental spectra are then composed using the random abundances mentioned above and corrupted by white Gaussian noise with variable signal-to-noise ratio. These simulated spectra would be the ones obtained ideally from a real measurement in the hypothesis of being able to perfectly subtract the continuum background B.

In figures 5 and 6, we show example MNF outputs, against noisy data with SNR=18 dB and SNR=42 dB, respectively. We cannot compare these results point by point with the original spectra, as the outputs are copies of the source functions up to scaling factors. For this reason, we rely on correlation coefficients. Since the LIBS spectra are strictly non-negative whereas the algorithm outputs can also assume negative values, we compute the correlation coefficients, r, between the original spectra and the positive values of the reconstructed ones.

In the case of 18 dB SNR, MNF produces 40 components, but only the first three correlate significantly with the ideal element spectra, while tin is not recovered at all ($r < 0.1$). Moreover, from the plot, it is well noticeable that the estimated copper spectrum contains residual components from the zinc. As we added Gaussian noise with equal variance to the spectra of all the 40 points, from a theoretical point of view PCA performs identically to MNF. Indeed, with PCA, copper and zinc are both recovered with correlation values similar to those of MNF, copper exhibits the same residual components from the zinc, tin is not recovered, and the estimated lead spectrum is even worse than the one obtained by MNF ($r = 0.192$).

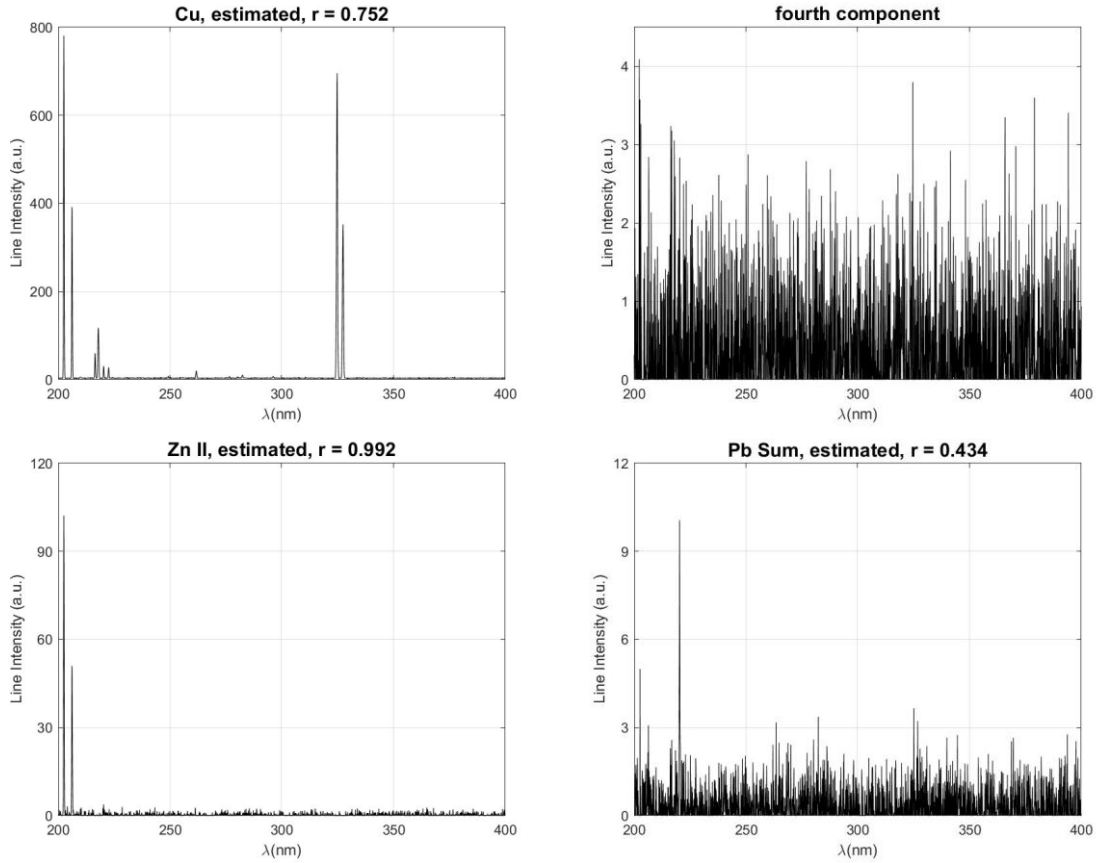

Figure 5 Elemental spectra estimated by MNF from data with Gaussian noise of 18 dB SNR.

For a noise of 42 dB the elemental spectra are recovered much better, and the noisiest component, the fourth one, this time has a correlation coefficient r=0.416 with the tin. However, copper still exhibits contaminations from the zinc, which, conversely, is recovered almost perfectly (r=1).

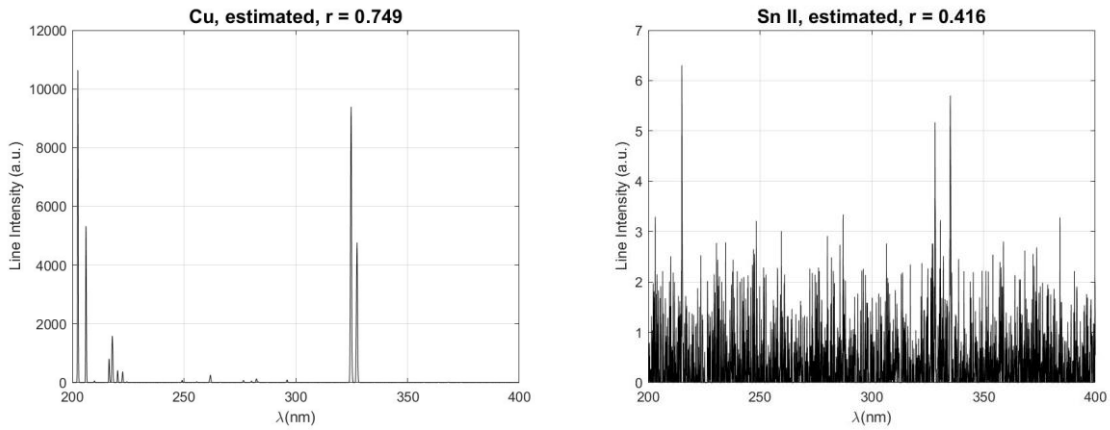

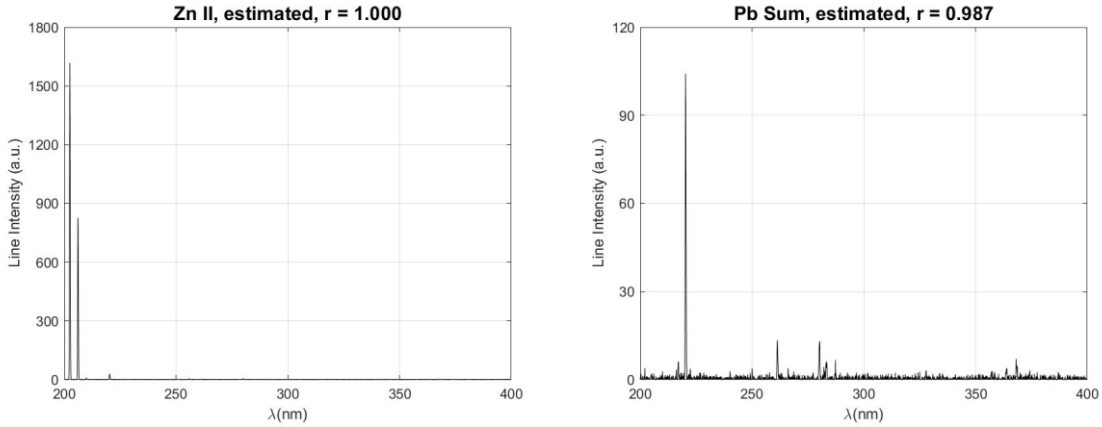

Figure 6 Elemental spectra estimated by MNF from data with Gaussian noise of 42 dB SNR.

The corresponding results from ICA are shown in Figs. 7 and 8. From Fig. 8, we note that the reconstructed tin spectrum has a very low correlation coefficient even with such a high SNR, so in practice tin is not extracted from the measured spectra. A possible reason for this is the small abundance of this analyte in the alloy under examination, as can be seen from the sample values in Tab. 2. In the case of Fig. 7, the ICA algorithm does not even evaluate the fourth component, since only three significant principal components are found (see below), and the correlation coefficient for the reconstructed lead spectrum is also quite low. Conversely, the reconstructed spectra of copper and zinc are still strongly correlated with the corresponding originals.

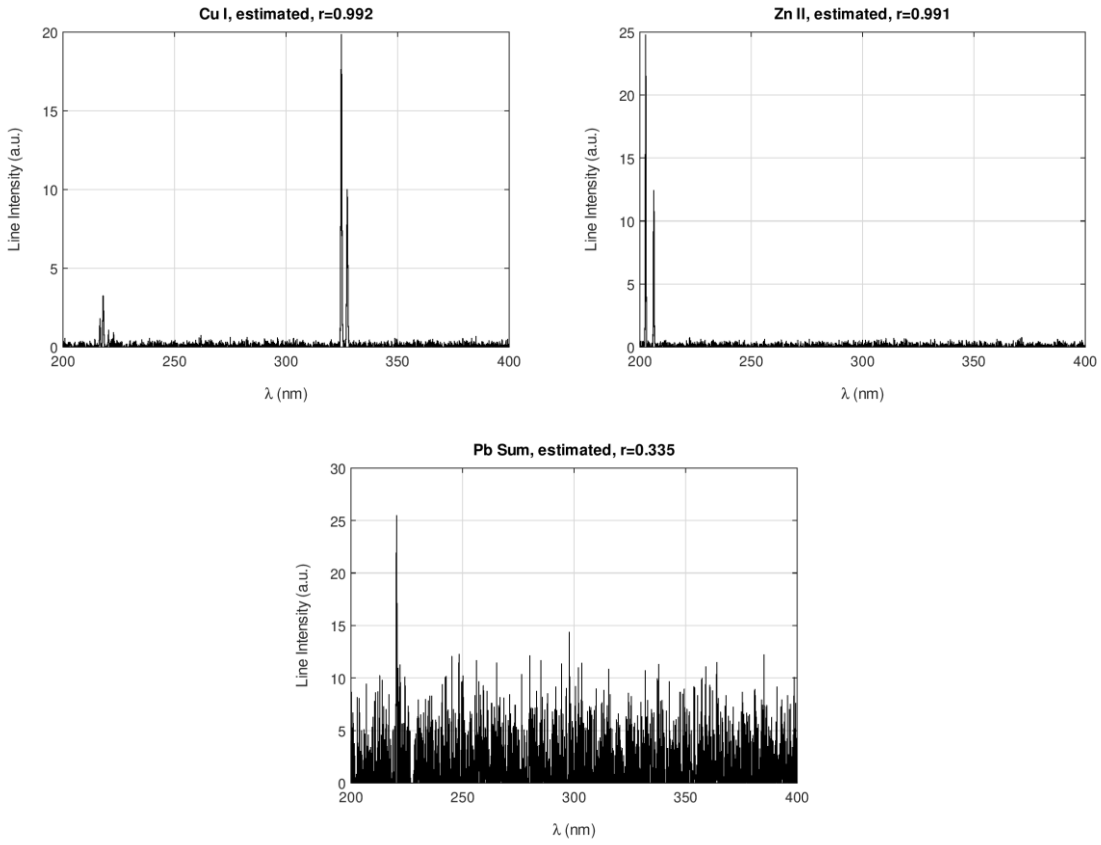

Figure 7 Elemental spectra estimated by ICA with Gaussian noise, 18 dB SNR. Only three outputs are computed, as the fourth eigenvalue of the data covariance matrix is equal or less than zero.

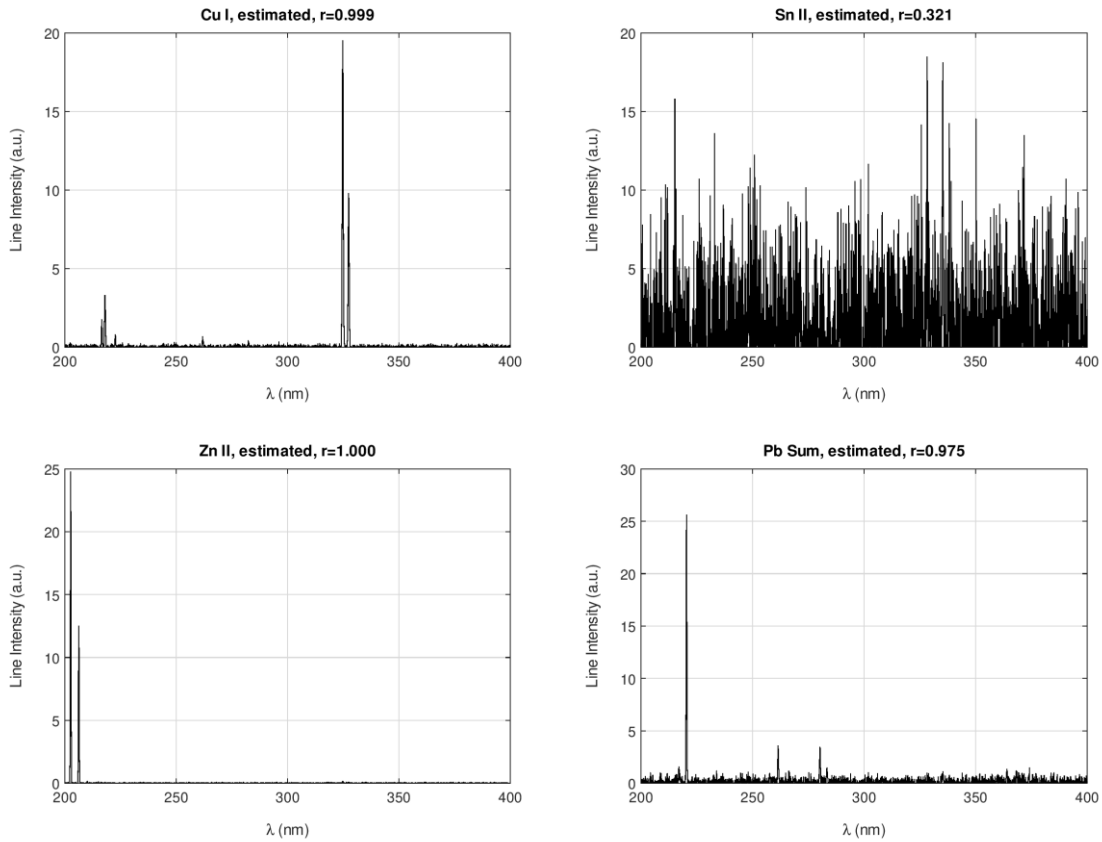

Figure 8 Elemental spectra estimated by ICA with Gaussian noise, 42 dB SNR.

To study the behaviour of ICA with different noise levels, we let them range from 60 to 12 dB in steps of 6 dB. The results are averaged over 10 runs of the algorithm to consider the variability of the noise realization and the fact that the initial guess for the solution of the separation problem is random. Table 3 reports the resulting correlation coefficients for all the reconstructed spectra, including, for comparison, the case of zero noise.

Table 3 Mean correlation coefficients between the elemental original and reconstructed spectra, with signals corrupted by white Gaussian additive noise.

Average correlation coefficients (10 runs)				
Noisy ICA		White, signal-independent Gaussian noise		
SNR (dB)	Cu I	Sn II	Zn II	Pb Sum
∞	0.99994	0.99996	0.99995	0.99992
60	0.99991	0.95533	0.99993	0.99961
54	0.99985	0.84880	0.99992	0.99861
48	0.99977	0.61573	0.99936	0.99454
42	0.99102	0.37058	0.99172	0.97925
36	0.89172	0.15477	0.95968	0.89317

30	0.9995960	-0.0024554	0.9994730	0.7874864
24	0.9984934	-0.0044540	0.9971295	0.5355158
18	0.9892834	0.0015834	0.9894578	0.3302940
12	0.9643751	0.0061326	0.9634158	0.2050567

Considering as well recovered the sources that correlate for more than an 80% with the corresponding outputs, it is easy to note that the copper and the zinc spectra are always recovered correctly, whereas the tin spectrum is very sensitive to noise and the lead spectrum is recovered correctly if the SNR is higher than 30 dB.

Following a suggestion by Hyvarinen (1999b), saying that the noisy version of ICA can also work with non-gaussian noise, we also tested this algorithm with data corrupted by multiplicative lognormal-distributed noise, as this is a natural choice for strictly positive measurements. We thus have coloured, signal-dependent noise.

Table 4 Mean correlation coefficients between the elemental original and reconstructed spectra, with signals corrupted by multiplicative lognormal noise.

Average correlation coefficients (10 runs)				
Noisy ICA		Multiplicative, lognormal-distributed noise		
SNR (dB)	Cu I	Sn II	Zn II	Pb Sum
∞	0.99994	0.99996	0.99995	0.99992
60	0.99734	0.96766	0.99888	0.99950
54	0.9999407	-0.0040305	0.9999168	0.9978723
48	0.9998225	-0.0045019	0.9998574	0.9924288
42	0.9998953	-0.0053434	0.9996803	0.9707330
36	0.9990394	-0.0062307	0.9985958	0.9257757
30	0.9994727	-0.0064664	0.9989289	0.0208064
24	0.9980711	-0.0067057	0.9973147	0.0197596
18	0.9928784	-0.0069262	0.9894208	0.0197565
12	0.9740855	-0.0075006	0.9688107	0.0166150

Also, in this case, although the data model used to design the separation algorithm includes Gaussian signal-independent noise, useful results are obtained. From Table 4, we see that copper and zinc are still reconstructed correctly for all the SNRs, and the lead spectrum is accurate for SNR>30 dB. The tin spectrum, conversely, is only recovered for SNR=60 dB.

Note that the ICA outputs reproduce the sources slightly better than the ones produced by MNF. Furthermore, the ICA outputs that correlate more than 0.8 with the corresponding elemental spectra do not present the spurious lines appearing in figs. 5 and 6. From tabs. 3 and 4, it is possible to note a

different behaviour of the ICA outputs with data affected by either signal-independent or signal-dependent noise. In the latter case, we have, for tin and lead, an abrupt transition between correlations well above 0.8 and very small values. This kind of values also appear in the results with Gaussian noise, except that the transitions are a little bit smoother. Following Hyvarinen (1999a, b), in our ICA algorithm, the data are first quasi-whitened and then rotated to maximize their mutual independence. In the presence of noise, the quasi-whitening matrix has the same form as in eq. (8), but it is even possible that some eigenvalue of order lower than N is zero. In this situation, ICA only produces less than N independent components. In our case (N=4), the estimation quality index for a given analyte is computed as the maximum correlation coefficient between its original spectrum and all the outputs. When less than 4 outputs are available, some original spectra (Sn II, Pb Sum, or both, in our case) will have all very small, meaningless, correlation values with all the outputs. Thus, the number of independent components computed as a function of the SNR can also be derived by just inspecting Tabs. 3 and 4. With Gaussian noise, ICA extracts only three independent components for SNR $\leq$ 30 dB whereas, for lognormal noise, ICA extracts only three components with SNR between 36 dB and 54 dB and only two components for SNR $\leq$ 30 dB.

7. Final Remarks

This short account of blind source separation methods for LIBS spectroscopy is mainly aimed at enabling the reader to understand the potentialities and the advantages offered by a correct isolation of the different elemental spectra in terms of 'readability' of the results. Indeed, the analysis by visual inspection of the individual spectra would be facilitated for the obtained separation of nearby lines belonging to different analytes and the consequent suppression of possible distortions due to line superposition. Also, some possibilities for an automatic spectrum analysis would be opened up, for example, if a dictionary of ideal elemental spectra were available, by computing their correlation coefficients with the algorithm outputs or, as often done with remote-sensed imagery, through the spectral angle mapping (SAM) technique (Kruse et al., 1993)

To our knowledge, this topic has not been explored thoroughly so far. Its complexity and promises, however, should encourage the research community to take it into account as a concrete possibility of improving the performance of LIBS analysis in many application fields. Many issues deserve to be addressed. First of all, an appropriate noise model would be helpful in both analyzing the behaviour of existing methods in front of different signal and noise situations, but also to try to develop separation methods that are specific to data affected by physically plausible noise and/or interference. Obviously, any algorithm would yield satisfactory results if the SNR is the least possible. This condition can be approached by either data pre-processing or accurate data capture, such as instrument calibration against systematic effects and the suppression of plasma-physics-associated phenomena.

As far as the study of theoretical/simulated performance is concerned, tabs. 3 and 4 above suggest the possibility to establish separability bounds as functions of the SNR and the composition of the material being examined, once a separability threshold is fixed (for example, r = 0.8, as above). Intuitively, an element whose relative abundance is small should need a very high SNR to be separated from the embedding spectra. Concrete results, however, let us conjecture that the number of independent measurement points also affects the separability, as well as the shape of an individual spectrum, the so-called 'skyline'. In our simulated experiments with complex metal alloys, the most abundant elements can be separated for any reasonably assumed SNR value, whereas the minor elements are not always separable.

While the results on simulated spectra seem promising, real experiments with measured LIBS spectra are still needed to assess the applicability of BSS methods to elemental spectra separation. In particular, the behaviour of these algorithms in the presence of interferences due to the physics of plasmas, such

as self-absorption, is not yet known. This means that an extensive experimentation is still needed to assess the possible added value provided by these techniques. It is to be noted, however, that BSS does not need to replace other well-established approaches. The results from this kind of technique could indeed support other results in particularly complicated cases, for example when no preliminary idea is available on the composition of the samples analyzed, thus helping a confident search for the significant spectral lines.

8. references

Alexander, D. R., Anderson, T., & Bruce, J. C., III (2012). *Laser Induced Breakdown Spectroscopy Having Enhanced Signal-to-Noise Ratio*. United States Patent Application Publication no. US 2012/0314214 A1, Dec. 13, 2012.

Bauer, H. E., Leis, F., & Niemax, K. (1998). Laser induced breakdown spectrometry with an echelle spectrometer and intensified charge coupled device detection. *Spectrochimica Acta Part B: Atomic Spectroscopy*, *53*(13), 1815–1825.

Bell, A. J., & Sejnowski, T. J. (1995a). An information-maximization approach to blind separation and blind deconvolution. *Neural Computation*, *7*(6), 1129–1159.

Bell, A. J., & Sejnowski, T. J. (1995b). Fast blind separation based on information theory. *Proc. Intern. Symp. on Nonlinear Theory and Applications, Las Vegas*.

Boué-Bigne, F. (2008). Laser-induced breakdown spectroscopy applications in the steel industry: Rapid analysis of segregation and decarburization. *Spectrochimica Acta - Part B Atomic Spectroscopy*, *63*(10), 1122–1129. https://doi.org/10.1016/j.sab.2008.08.014

Bulajic, D., Corsi, M., Cristoforetti, G., Legnaioli, S., Palleschi, V., Salvetti, A., & Tognoni, E. (2002). A procedure for correcting self-absorption in calibration free-laser induced breakdown spectroscopy. Spectrochimica Acta Part B: Atomic Spectroscopy, 57(2), 339–353.

Busser, B., Moncayo, S., Coll, J.-L., Sancey, L., & Motto-Ros, V. (2018). Elemental imaging using laser-induced breakdown spectroscopy: A new and promising approach for biological and medical applications. *Coordination Chemistry Reviews*, *358*, 70–79. https://doi.org/10.1016/j.ccr.2017.12.006

Carvalho, R. R. V, Coelho, J. A. O., Santos, J. M., Aquino, F. W. B., Carneiro, R. L., & Pereira-Filho, E. R. (2015). Laser-induced breakdown spectroscopy (LIBS) combined with hyperspectral imaging for the evaluation of printed circuit board composition. *Talanta*, *134*, 278–283. https://doi.org/10.1016/j.talanta.2014.11.019

Casado-Gavalda, M. P., Dixit, Y., Geulen, D., Cama-Moncunill, R., Cama-Moncunill, X., Markiewicz-Keszycka, M., Cullen, P. J., & Sullivan, C. (2017). Quantification of copper content with laser induced breakdown spectroscopy as a potential indicator of offal adulteration in beef. *Talanta*, *169*, 123–129. https://doi.org/10.1016/j.talanta.2017.03.071

Choi, S., Cichocki, A., Park, H.-M., & Lee, S.-Y. (2005). Blind source separation and independent component analysis: A review. *Neural Information Processing-Letters and Reviews*, *6*(1), 1–57.

Cichocki, A., & Amari, S. (2002). *Adaptive blind signal and image processing: learning algorithms and applications*. John Wiley & Sons.

Dabiri, Z., & Lang, S. (2018). Comparison of independent component analysis, principal component analysis, and minimum noise fraction transformation for tree species classification using APEX hyperspectral imagery. *ISPRS International Journal of Geo-Information*, *7*(12), 488.

Danzer, K. (1984). Comparison of sampling procedures for investigation of chemical homogeneity of solids by spark emission spectrography. *Spectrochimica Acta Part B: Atomic Spectroscopy*, *39*(8), 949–954.

Dixit, Y., Casado-Gavalda, M. P., Cama-Moncunill, R., Cama-Moncunill, X., Markiewicz-Keszycka, M., Cullen, P. J., & Sullivan, C. (2017). Laser induced breakdown spectroscopy for quantification of sodium and potassium in minced beef: A potential technique for detecting beef kidney adulteration. *Analytical Methods*, *9*(22), 3314–3322. https://doi.org/10.1039/c7ay00757d

Fabre, C., Devismes, D., Moncayo, S., Pelascini, F., Trichard, F., Lecomte, A., Bousquet, B., Cauzid, J., & Motto-Ros, V. (2018). Elemental imaging by laser-induced breakdown spectroscopy for the geological characterization of minerals. *Journal of Analytical Atomic Spectrometry*, *33*(8), 1345–1353. https://doi.org/10.1039/c8ja00048d

Fortes, F. J., Perez-Carceles, M. D., Sibon, A., Luna, A., & Laserna, J. J. (2015). Spatial distribution analysis of strontium in human teeth by laser-induced breakdown spectroscopy: application to diagnosis of seawater drowning. *International Journal of Legal Medicine*, *129*(4), 807–813. https://doi.org/10.1007/s00414-014-1131-9

Fu, Y., Hou, Z., Li, T., Li, Z., & Wang, Z. (2019). Investigation of intrinsic origins of the signal uncertainty for laser-induced breakdown spectroscopy. *Spectrochimica Acta Part B: Atomic Spectroscopy*, *155*, 67–78.

Gao, L., Zhao, B., Jia, X., Liao, W., & Zhang, B. (2017). Optimized kernel minimum noise fraction transformation for hyperspectral image classification. *Remote Sensing*, *9*(6), 548.

Gimenez, Y., Busser, B., Trichard, F., Kulesza, A., Laurent, J. M., Zaun, V., Lux, F., Benoit, J. M., Panczer, G., Dugourd, P., Tillement, O., Pelascini, F., Sancey, L., & Motto-Ros, V. (2016). 3D Imaging of Nanoparticle Distribution in Biological Tissue by Laser-Induced Breakdown Spectroscopy. *Scientific Reports*, *6*. https://doi.org/10.1038/srep29936

Green, A. A., Berman, M., Switzer, P., & Craig, M. D. (1988). A transformation for ordering multispectral data in terms of image quality with implications for noise removal. *IEEE Transactions on Geoscience and Remote Sensing*, *26*(1), 65–74.

Häkkänen, H. J., & Korppi-Tommola, J. E. I. (1995). UV-laser plasma study of elemental distributions of paper coatings. *Appl. Spectrosc.*, *49*(12), 1721–1728.

Harris, J. R., Rogge, D., Hitchcock, R., Ijewliw, O., & Wright, D. (2005). Mapping lithology in Canada's Arctic: application of hyperspectral data using the minimum noise fraction transformation and matched filtering. *Canadian Journal of Earth Sciences*, *42*(12), 2173–2193.

Hausmann, N., Siozos, P., Lemonis, A., Colonese, A. C., Robson, H. K., & Anglos, D. (2017). Elemental mapping of Mg/Ca intensity ratios in marine mollusc shells using laser-induced breakdown spectroscopy. *Journal of Analytical Atomic Spectrometry*, *32*(8), 1467–1472. https://doi.org/10.1039/c7ja00131b

Hoehse, M., Gornushkin, I., Merk, S., & Panne, U. (2011). Assessment of suitability of diode pumped solid state lasers for laser induced breakdown and Raman spectroscopy. *Journal of Analytical Atomic Spectrometry*, *26*(2), 414–424. https://doi.org/10.1039/c0ja00038h

Hong, S., Lai, W. W.-L., Wilsch, G., Helmerich, R., Helmerich, R., Günther, T., & Wiggenhauser, H. (2014). Periodic mapping of reinforcement corrosion in intrusive chloride contaminated concrete with GPR. *Construction and Building Materials*, *66*, 671–684. https://doi.org/10.1016/j.conbuildmat.2014.06.019

Hyvarinen, A. (1999a). Fast and robust fixed-point algorithms for independent component analysis. *IEEE Transactions on Neural Networks*, *10*(3), 626–634.

Hyvarinen, A. (1999b). Gaussian moments for noisy independent component analysis. *IEEE Signal Processing Letters*, *6*(6), 145–147.

Hyvarinen, A. (1999c). Fast ICA for noisy data using Gaussian moments. *1999 IEEE International Symposium on Circuits and Systems (ISCAS)*, *5*, 57–61.

Hyvärinen, A, Karhunen, J., & Oja, E. (2001). al. Independent component analysis. John Wiley and Sons. *Inc., New York*.

Hyvärinen, A. (2001). Fast ICA by a fixed-point algorithm that maximizes non-Gaussianity. *Independent Component Analysis: Principles and Practice*, *1*.

Hyvärinen, A, & Oja, E. (1997). A fast fixed-point algorithm for independent component analysis. *Neural Computation*, *9*(7), 1483–1492.

Jain, S. N., & Rai, C. (2012). Blind source separation and ICA techniques: a review. *IJEST*, *4*(4), 1490–1503.

Karhunen, J., & Joutsensalo, J. (1994). Representation and separation of signals using nonlinear PCA type learning. *Neural Networks*, *7*(1), 113–127.

Karhunen, J., Pajunen, P., & Oja, E. (1998). The nonlinear PCA criterion in blind source separation: Relations with other approaches. *Neurocomputing*, *22*(1–3), 5–20.

Karhunen, J., Wang, L., & Vigario, R. (1995). Nonlinear PCA type approaches for source separation and independent component analysis. *Proceedings of ICNN'95-International Conference on Neural Networks*, *2*, 995–1000.

Kempenaers, L., Janssens, K., Vincze, L., Vekemans, B., Somogyi, A., Drakopoulos, M., Simionovici, A., & Adams, F. (2002). A Monte Carlo model for studying the microheterogeneity of trace elements in reference materials by means of synchrotron microscopic X-ray fluorescence. *Analytical Chemistry*, *74*(19), 5017–5026.

Kim, T., Lin, C. T., & Yoon, Y. (1998). Compositional mapping by laser-induced breakdown spectroscopy. *Journal of Physical Chemistry B*, *102*(22), 4284–4287.

Kruse, F. A., Lefkoff, A. B., Boardman, J. W., Heidebrecht, K. B., Shapiro, A. T., Barloon, P. J., & Goetz, A. F. H. (1993). The spectral image processing system (SIPS)-interactive visualization and analysis of imaging spectrometer data. AIP Conference Proceedings, 283(1), 192–201.

Le Guével, X., Henry, M., Motto-Ros, V., Longo, E., Montañez, M. I., Pelascini, F., De La Rochefoucauld, O., Zeitoun, P., Coll, J.-L., Josserand, V., & Sancey, L. (2018). Elemental and optical imaging evaluation of zwitterionic gold nanoclusters in glioblastoma mouse models. *Nanoscale*, *10*(39), 18657–18664. https://doi.org/10.1039/c8nr05299a

Lednev, V. N., Sdvizhenskii, P. A., Grishin, M. Y. A., Cheverikin, V. V, Stavertiy, A. Y. A., Tretyakov, R. S., Taksanc, M. V, & Pershin, S. M. (2017). Laser-induced breakdown spectroscopy for three-dimensional elemental mapping of composite materials synthesized by additive technologies. *Applied Optics*, *56*(35), 9698–9705. https://doi.org/10.1364/AO.56.009698

Lee, J. B., Woodyatt, A. S., & Berman, M. (1990). Enhancement of high spectral resolution remote-sensing data by a noise-adjusted principal components transform. *IEEE Transactions on Geoscience and Remote Sensing*, *28*(3), 295–304.

Lefebvre, C., Catalá-Espí, A., Sobron, P., Koujelev, A., & Léveillé, R. (2016). Depth-resolved chemical mapping of rock coatings using Laser-Induced Breakdown Spectroscopy: Implications for geochemical investigations on Mars. *Planetary and Space Science*, *126*, 24–33. https://doi.org/10.1016/j.pss.2016.04.003

Li, J., Hao, Z., Zhao, N., Zhou, R., Yi, R., Tang, S., Guo, L., Li, X., Zeng, X., & Lu, Y. (2017). Spatially selective excitation in laser-induced breakdown spectroscopy combined with laser-induced fluorescence. *Optics Express*, *25*(5), 4945–4951. https://doi.org/10.1364/OE.25.004945

Lin, Q.-H., Zheng, Y.-R., Yin, F.-L., Liang, H., & Calhoun, V. D. (2007). A fast algorithm for one-unit ICA-R. *Information Sciences*, *177*(5), 1265–1275.

López-López, M., Alvarez-Llamas, C., Pisonero, J., García-Ruiz, C., & Bordel, N. (2017). An exploratory study of the potential of LIBS for visualizing gunshot residue patterns. *Forensic Science International*, *273*. https://doi.org/10.1016/j.forsciint.2017.02.012

Lopez-Quintas, I., Mateo, M. P., Piñon, V., Yañez, A., & Nicolas, G. (2012). Mapping of mechanical specimens by laser induced breakdown spectroscopy method: Application to an engine valve. *Spectrochimica Acta - Part B Atomic Spectroscopy*, *74–75*, 109–114. https://doi.org/10.1016/j.sab.2012.06.035

Luo, G., Chen, G., Tian, L., Qin, K., & Qian, S.-E. (2016). Minimum noise fraction versus principal component analysis as a preprocessing step for hyperspectral imagery denoising. *Canadian Journal of Remote Sensing*, *42*(2), 106–116.

Mermet, J. M., Mauchien, P., & Lacour, J. L. (2008). Processing of shot-to-shot raw data to improve precision in laser-induced breakdown spectrometry microprobe. *Spectrochimica Acta Part B: Atomic Spectroscopy*, *63*(10), 999–1005.

Motto-Ros, V., Moncayo, S., Trichard, F., & Pelascini, F. (2019). Investigation of signal extraction in the frame of laser induced breakdown spectroscopy imaging. Spectrochimica Acta Part B: Atomic Spectroscopy, 155, 127–133.

Motto-Ros, V., Sancey, L., Ma, Q. L., Lux, F., Bai, X. S., Wang, X. C., Yu, J., Panczer, G., & Tillement, O. (2012). Mapping of native inorganic elements and injected nanoparticles in a biological organ with laser-induced plasma. *Applied Physics Letters*, *101*(22). https://doi.org/10.1063/1.4768777

Noll, R., Bette, H., Brysch, A., Kraushaar, M., Mönch, I., Peter, L., & Sturm, V. (2001). Laser-induced breakdown spectrometry - Applications for production control and quality assurance in the steel industry. *Spectrochimica Acta - Part B Atomic Spectroscopy*, *56*(6), 637–649. https://doi.org/10.1016/S0584-8547(01)00214-2

Oja, E. (1995). *The nonlinear PCA learning rule and signal separation: Mathematical analysis*. Helsinki University of Technology Espoo, Finland.

Oja, E., & Plumbley, M. (2003). Blind separation of positive sources using non-negative PCA. *4th International Symposium on Independent Component Analysis and Blind Signal Separation*.

Pagnotta, S., Lezzerini, M., Ripoll-Seguer, L., Hidalgo, M., Grifoni, E., Legnaioli, S., Lorenzetti, G., Poggialini, F., & Palleschi, V. (2017). Micro-Laser-Induced Breakdown Spectroscopy (Micro-LIBS) Study on Ancient Roman Mortars. *Applied Spectroscopy*, *71*(4), 721–727.

Pajunen, P., & Karhunen, J. (1997). Least-squares methods for blind source separation based on nonlinear PCA. *International Journal of Neural Systems*, *8*(05n06), 601–612.

Pal, M., Roy, R., Basu, J., & Bepari, M. S. (2013). Blind source separation: A review and analysis. *2013 International Conference Oriental COCOSDA Held Jointly with 2013 Conference on Asian Spoken Language Research and Evaluation (O-COCOSDA/CASLRE)*, 1–5.

Peng, J., Liu, F., Zhou, F., Song, K., Zhang, C., Ye, L., & He, Y. (2016). Challenging applications for multi-element analysis by laser-induced breakdown spectroscopy in agriculture: A review. *TrAC - Trends in Analytical Chemistry*, *85*, 260–272. https://doi.org/10.1016/j.trac.2016.08.015

Rifai, K., Doucet, F., Özcan, L., & Vidal, F. (2018). LIBS core imaging at kHz speed: Paving the way for real-time geochemical applications. *Spectrochimica Acta - Part B Atomic Spectroscopy*, *150*, 43–48. https://doi.org/10.1016/j.sab.2018.10.007

Roger, R. E. (1994). A faster way to compute the noise-adjusted principal components transform matrix. *IEEE Transactions on Geoscience and Remote Sensing*, *32*(6), 1194–1196.

Romero, D., & Laserna, J. J. (1997). Multielemental Chemical Imaging Using Laser-Induced Breakdown Spectrometry. *Analytical Chemistry*, *69*(15), 2871–2876. https://doi.org/10.1021/ac9703111

Sallé, B., Lacour, J.-L., Mauchien, P., Fichet, P., Maurice, S., & Manhes, G. (2006). Comparative study of different methodologies for quantitative rock analysis by laser-induced breakdown spectroscopy in a simulated Martian atmosphere. *Spectrochimica Acta Part B: Atomic Spectroscopy*, *61*(3), 301–313.

Schiavo, C., Menichetti, L., Grifoni, E., Legnaioli, S., Lorenzetti, G., Poggialini, F., Pagnotta, S., & Palleschi, V. (2016). High-resolution three-dimensional compositional imaging by double-pulse laser-induced breakdown spectroscopy. *Journal of Instrumentation*, *11*(08), C08002.

Schlenke, J., Hildebrand, L., Moros, J., & Laserna, J. J. (2012). Adaptive approach for variable noise suppression on laser-induced breakdown spectroscopy responses using stationary wavelet transform. *Analytica Chimica Acta*, *754*, 8–19.

Sheta, S. A., Di Carlo, G., Ingo, G. M., & Harith, M. A. (2015). Surface heterogeneity study of some reference Cu-Ag alloys using laser-induced breakdown spectroscopy. *Surface and Interface Analysis*, *47*(4), 514–522. https://doi.org/10.1002/sia.5741

Škarková, P., Novotný, K., Lubal, P., Jebavá, A., Pořízka, P., Klus, J., Farka, Z., Hrdlička, A., & Kaiser, J. (2017). 2d distribution mapping of quantum dots injected onto filtration paper by laser-induced breakdown spectroscopy. *Spectrochimica Acta - Part B Atomic Spectroscopy*, *131*, 107–114. https://doi.org/10.1016/j.sab.2017.03.016

Sperança, M. A., de Aquino, F. W. B., Fernandes, M. A., Lopez-Castillo, A., Carneiro, R. L., & Pereira-Filho, E. R. (2017). Application of Laser-Induced Breakdown Spectroscopy and Hyperspectral Images for Direct Evaluation of Chemical Elemental Profiles of Coprolites. *Geostandards and Geoanalytical Research*, *41*(2), 273–282. https://doi.org/10.1111/ggr.12155

St-Onge, L., Detalle, V., & Sabsabi, M. (2002). Enhanced laser-induced breakdown spectroscopy using the combination of fourth-harmonic and fundamental Nd: YAG laser pulses. *Spectrochimica Acta Part B: Atomic Spectroscopy*, *57*(1), 121–135.

Sun, Y. (2005). The study and test of ICA algorithms. *Proceedings. 2005 International Conference on Wireless Communications, Networking and Mobile Computing, 2005.*, *1*, 602–605.

Sun, L., & Yu, H. (2009). Automatic estimation of varying continuum background emission in laser-induced breakdown spectroscopy. Spectrochimica Acta Part B: Atomic Spectroscopy, 64(3), 278–287.

Taparli, U. A., Jacobsen, L., Griesche, A., Michalik, K., Mory, D., & Kannengiesser, T. (2018). In situ laser-induced breakdown spectroscopy measurements of chemical compositions in stainless steels during tungsten inert gas welding. *Spectrochimica Acta - Part B Atomic Spectroscopy*, *139*, 50–56. https://doi.org/10.1016/j.sab.2017.11.012

Tognoni, E., & Cristoforetti, G. (2016). Signal and noise in laser induced breakdown spectroscopy: an introductory review. Optics & Laser Technology, 79, 164–172.

Tognoni, E., Palleschi, V., Corsi, M., & Cristoforetti, G. (2002). Quantitative micro-analysis by laser-induced breakdown spectroscopy: a review of the experimental approaches. Spectrochimica Acta Part B: Atomic Spectroscopy, 57(7), 1115–1130.

Trichard, F., Gaulier, F., Barbier, J., Espinat, D., Guichard, B., Lienemann, C.-P., Sorbier, L., Levitz, P., & Motto-Ros, V. (2018). Imaging of alumina supports by laser-induced breakdown spectroscopy: A new tool to understand the diffusion of trace metal impurities. *Journal of Catalysis*, *363*, 183–190. https://doi.org/10.1016/j.jcat.2018.04.013

Wiggins, B., Tupitsyn, E., Bhattacharya, P., Rowe, E., Lukosi, E., Chvala, O., Burger, A., & Stowe, A. (2013). Investigation of non-uniformity and inclusions in 6LiInSe 2 utilizing laser induced breakdown spectroscopy (LIBS). *Proceedings of SPIE - The International Society for Optical Engineering*, *8852*. https://doi.org/10.1117/12.2024125

Xu, L., Bulatov, V., Gridin, V. V, & Schechter, I. (1997). Absolute analysis of particulate materials by laser-induced breakdown spectroscopy. Analytical Chemistry, 69(11), 2103–2108.

Xu, T., Liu, J., Shi, Q., He, Y., Niu, G., & Duan, Y. (2016). Multi-elemental surface mapping and analysis of carbonaceous shale by laser-induced breakdown spectroscopy. *Spectrochimica Acta - Part B Atomic Spectroscopy*, *115*, 31–39. https://doi.org/10.1016/j.sab.2015.10.008

Yaroshchyk, P., & Eberhardt, J. E. (2014). Automatic correction of continuum background in Laser-induced Breakdown Spectroscopy using a model-free algorithm. *Spectrochimica Acta Part B: Atomic Spectroscopy*, 99, 138–149. https://doi.org/10.1016/j.sab.2014.06.020

Zhang, B., Sun, L., Yu, H., Xin, Y., & Cong, Z. (2013). Wavelet denoising method for laser-induced breakdown spectroscopy. *Journal of Analytical Atomic Spectrometry*, *28*(12), 1884–1893.

Zhang, B., Sun, L., Yu, H., Xin, Y., & Cong, Z. (2015). A method for improving wavelet threshold denoising in laser-induced breakdown spectroscopy. *Spectrochimica Acta Part B: Atomic Spectroscopy*, *107*, 32–44.

Zhu, X.-L., Zhang, X.-D., Ding, Z.-Z., & Jia, Y. (2006). Adaptive nonlinear PCA algorithms for blind source separation without prewhitening. *IEEE Transactions on Circuits and Systems I: Regular Papers*, *53*(3), 745–753.

Zou, X. H., Guo, L. B., Shen, M., Li, X. Y., Hao, Z. Q., Zeng, Q. D., Lu, Y. F., Wang, Z. M., & Zeng, X. Y. (2014). Accuracy improvement of quantitative analysis in laser-induced breakdown spectroscopy using modified wavelet transform. *Optics Express*, *22*(9), 10233–10238.